ELSEVIER

Journal of Molecular Catalysis A: Chemical 161 (2000) 49–64

JOURNAL OF MOLECULAR CATALYSIS A: CHEMICAL

www.elsevier.com/locate/molcata

Formation and role of cobalt and manganese cluster complexes in the oxidation of *p*-xylene

S.A. Chavan, S.B. Halligudi, D. Srinivas, P. Ratnasamy *

National Chemical Laboratory, Pune 411008, India

Received 24 May 2000; accepted 19 June 2000

Abstract

The mono- and multinuclear metal complexes present during the aerial oxidation of *p*-xylene by the homogeneous catalyst systems viz. Co/Br, Mn/Br, Co/Mn/Br, Co/Ce/Br, Co/Zr/Br, Co/Mn/Zr/Br, Co/Mn/Ce/Br, Ni/Mn/Br and Ni/Mn/Zr/Br in acetic acid solvent have been investigated by electronic and EPR spectroscopies. The reaction mixtures contain, in addition to $Co(OAc)_2 \cdot 4H_2O$ and $Mn(OAc)_2 \cdot 4H_2O$, species like Co(OAc)Br, $Co(OAc)_3$, $Co_3(O)(OAc)_x$, $Mn_3(O)(OAc)_x$ and hetero-multinuclear complexes like $Co_2Mn(O)(OAc)_x$ and $CoMn_2(O)(OAc)_x$. While mononuclear $Co(OAc)_2$, $Mn(OAc)_2$ and Co(OAc)Br complexes predominate in the initial stages of the oxidation reaction, significant concentrations of multinuclear Co(III) and Mn(III) complexes are detected in the later stages. Zr(IV), when present, facilitates the oxidation of Mn(II) to Mn(III), a crucial step in the kinetic pathway of the oxidation reaction. Our EPR results indicate the presence of homo-nuclear $Mn_3(O)(OAc)_x$ type clusters as the major species with a minor component of $CoMn_2(O)(OAc)_x$ complex in catalyst systems with Co:Mn = 1:3 (mol). When an excess of cobalt catalyst is used (e.g. Co:Mn = 3:1) or when Zr and Br^- are also present in optimal concentrations, the heteronuclear cluster $Co_2Mn(O)(OAc)_x$ predominates while $Co_3(O)(OAc)_x$ and $CoMn_2(O)(OAc)_x$ occur as minor constituents. The yield of terephthalic acid (TA) is enhanced at high concentrations of cluster complexes like $Co_2Mn(O)(OAc)_x$ and $CoMn_2(O)(OAc)_x$. The combination Co/Mn/Zr (3:1:0.1 mol), exhibits a high catalytic activity and selectivity for terephthalic acid, especially in the presence of an optimal concentration of the bromide ion.

Keywords: Oxidation of *p*-xylene; Co/Mn/Br^- catalyst; Electronic spectroscopy; EPR spectroscopy; Cluster complexes of cobalt and manganese; Terephthalic acid

1. Introduction

Terephthalic acid (TA), one of the largest volume commodity chemicals obtained by selective oxidation, is commercially manufactured by the dioxygen oxidation of *p*-xylene (PX) using a catalyst combination of cobalt and manganese salts and a bromide ion promoter in acetic acid (HOAc) medium at 443–483 K. The commercial process has been optimized to the point where typical crude TA purities of 98–99.5% are produced in yields of 96–97 mol% based on PX feed at an oxidizer contact time of 45–90 min [1,2]. However, the following three improvements are desirable in the existing process: (i)

* Corresponding author. Tel.: +91-20-5893030; fax: 91-20-5893355.

E-mail address: prs@ems.ncl.res.in (P. Ratnasamy).

1381-1169/00/$ - see front matter
PII: S1381-1169(00)00361-7

reduction or elimination of the significant HOAc oxidation to CO and CO_2 (5–10 wt.% of TA); this can perhaps be achieved by the use of more efficient radical promoters which allow oxidizer temperatures to be lowered without reducing reaction rates, (ii) alternatives to the highly corrosive HOAc and bromide ion promoters which require the use of expensive titanium steel, and (iii) reduction or elimination of the 4-carboxybenzaldehyde (4-CBA) and other impurities from crude TA which necessitate elaborate hydrogenation and recrystallization procedures in the manufacture of purified TA required for the polyester industry.

A better understanding of the *chemistry* of the catalyst system is essential to achieve the above process improvements. Surprisingly, even though the kinetics of the reaction network and the process engineering aspects of the manufacture of TA has been thoroughly investigated [3–17], there are comparatively fewer studies devoted to the identity and role of the catalytically active cobalt and manganese species involved in the complex series of reactions in the conversion of PX to TA [18–20]. Similarly, the roles of the promoter Br^-, the solvent HOAc and other additives used in the industrial process, are also not well understood. The mechanism is believed to begin with hydrogen atom abstraction from the methyl group by the bromine atom. The resultant benzyl radical adds to O_2 and proceeds through the hydroperoxide to *p*-tolyl alcohol, *p*-tolyl aldehyde and *p*-toluic acid. Hydrogen atom abstraction from the methyl group in *p*-toluic acid generates a secondary benzyl radical, which follows the same pathway to yield eventually, TA.

The transition metals (Co and Mn) are believed to be responsible for the chain initiation, propagation and decomposition of various peroxides formed during the reaction as well as the conversion of Br^- to $Br^{\cdot}$ [8,9]. The active forms of cobalt and manganese in the systems, however, are still not established with certainty although several mononuclear, Co(OAc)Br [9,15], binuclear, $[Co_2(OH)_2(OAc)_4]$ [20,21] and trinuclear, $[Co_3O(OAc)_5(OH)(HOAc)_3]$ [20,21] and $[Co_3O(OAc)_5(HOAc)_3]$, [22–25] complexes have been proposed. It is probable that the identity, concentrations and role of these complexes depend on the Co/Mn, Br/Co and Co/HOAc ratios, presence of additives like Zr and Ce [2] as well as the process conditions like temperature, pressure, concentration of dioxygen etc.

The major objective of the present study is to investigate, using electronic and electron paramagnetic resonance (EPR) spectroscopies, the cobalt and manganese species that are formed during the dioxygen oxidation of PX over the Co and Mn catalyst system. The influence of additives like Zr, Ce and Ni, on the rates of oxidation, product distribution and EPR spectra has also been explored. The catalysis data are supplemented by performing in situ electronic and EPR spectral measurements. These spectroscopic techniques are complementary, powerful to detect even trace quantities of various species present in the reaction medium and provide a deeper insight into the structure of the active catalytic species [26]. Mn(II) is paramagnetic ($3d^5$, $S = 5/2$) and shows a resolved hyperfine pattern in the EPR spectrum even at room temperature. The hyperfine splitting and other spin Hamiltonian parameters are sensitive to the symmetry and molecular environment. But Mn(II) does not show any d–d bands in the electronic spectrum due to the $^6A_{1g}$ ground state and transition to excited states are spin forbidden [27]. Mn(III), on the other hand, shows characteristic electronic spectral features but is EPR silent. The Co(II) ion is also paramagnetic ($3d^7$, $S = 3/2$), but due to the short spin-lattice relaxation times, its EPR signals cannot be detected at ambient temperatures and the measurements need to be performed at liquid helium temperatures [28]. However, both Co(II) and Co(III) exhibit distinct electronic spectra even at room temperature [12,15]. Thus a combined study using both electronic and EPR spectroscopies can yield significant insight into the identity and role of Co and Mn species that are formed during the oxidation reaction. To our knowledge, a detailed EPR spectroscopic study of this catalyst system and the influence of Zr and Ni and bromide promoter have not been published, so far.

2. Experimental

2.1. Materials

$Co(OAc)_2 \cdot 4H_2O$, $Mn(OAc)_2 \cdot 4H_2O$, $Ni(OAc)_2 \cdot 4H_2O$, $Ce(NO_3)_3 \cdot 6H_2O$, $ZrOCl_2 \cdot xH_2O$ and NaBr were procured from M/S Loba Chemicals.

$Zr(OH)_4$ was prepared from $ZrOCl_2 \cdot xH_2O$ by interacting with NH_4OH. Terephthalic acid, *p*-xylene, *p*-toluic acid, dimethylterephthalate and pyridine were obtained from Aldrich. High purity grade glacial acetic acid (97%) was used in the *p*-xylene oxidation experiments. Air, as the source of oxygen, was bubbled through the glass reactor using an air compressor.

2.2. Spectroscopic measurements

The UV–VIS spectra were recorded on a Perkin-Elmer UV-101 PC scanning spectrophotometer, in the region 200–800 nm. EPR spectra were measured on a Bruker EMX spectrometer operating at X-band frequency ($\nu = 9.75$ GHz) and 100 kHz field modulation. Frequency calibration was done using a frequency counter fitted with a ER 041 XG-D microwave bridge. The magnetic field was calibrated using a Bruker ER 035 M NMR Gaussmeter. For measurements at 298 K, the liquid samples were taken in a quartz aqueous cell. The measurements at 77 K were performed using a quartz finger Dewar (Bruker ER 167 FDS-Q). Spectral manipulations were done using a Bruker WINEPR software package. To record the UV–VIS and EPR spectra of reaction mixtures, a known amount of liquid sample was taken out from the reaction vessel and quenched to 298 or 77 K.

2.3. Reaction procedure and product analysis

An U-shaped, bubble-column glass reactor (100 ml volume) fitted with standard joints and having a sintered glass disc gas distributor fixed at the bottom of the reactor was placed in an oil bath and maintained at 363 K. Air was bubbled into the reactor through the sintered glass disc. The glass reactor was also fitted with water condenser, through which, water at 280 K was circulated.

In a sample run, known amounts of PX, metal salts ($Co(OAc)_2 \cdot 4H_2O$, $Mn(OAc)_2 \cdot 4H_2O$, etc.), NaBr, water, HOAc were mixed in the reactor at 363 K. Air from the compressor was bubbled through the reactor at a rate of 50 ml/min. At the end of the run, the reaction mixture was rapidly cooled to 298 K. Mass balances were calculated from the weights of the reaction mixture before and after the reaction. After separating the solids, liquid products and unreacted PX were analyzed by gas chromatography (Shimadzu, GC-14B with a 6 ft 10% SE-30 S. S. packed column, 1/8 in. O.D., and FID detector). The total reaction mixture was, then, distilled under vacuum to remove HOAc, water and unreacted PX. The solid mass obtained was washed with hot water to remove the water-soluble catalyst salts. The solid products (*p*-toluic acid, 4-CBA and TA), thus obtained, were dried in an oven and their weights were recorded. The solid products were esterified by known methods using BF_3 in methanol solution [29]. The esters were again analyzed by gas chromatography. Products were identified by GCMS (Shimadzu QP 5000).

3. Results and discussion

3.1. Electronic spectroscopy

Electronic spectral studies were carried out on the following homogeneous solutions.

(a) $Co(OAc)_2 \cdot 4H_2O$ (1.03 mmol)/NaBr (1.35 mmol)/HOAc (587 mmol)/H_2O (311 mmol)/air.

(b) $Co(OAc)_2 \cdot 4H_2O$ (1.03 mmol)/NaBr (1.35 mmol)/HOAc (587 mmol)/H_2O (311 mmol)/PX (44.3 mmol)/air.

(c) $Co(OAc)_2 \cdot 4H_2O$ (1.03 mmol)/$Mn(OAc)_2 \cdot 4H_2O$ (0.35 mmol)/NaBr (1.35 mmol)/HOAc (587 mmol)/H_2O (311 mmol)/PX (44.3 mmol)/air.

(d) $Co(OAc)_2 \cdot 4H_2O$ (1.03 mmol)/$Mn(OAc)_2 \cdot 4H_2O$ (0.35 mmol)/NaBr (1.35 mmol)/HOAc (587 mmol)/H_2O (311 mmol)/PX (44.3 mmol)/H_2O_2.

(e) $Mn(OAc)_2 \cdot 4H_2O$ (1.03 mmol)/NaBr (1.35 mmol)/HOAc (587 mmol)/H_2O (311 mmol)/PX (44.3 mmol)/air.

A known amount of solution was taken out from the reaction vessel (which was maintained at 363 K), at specified times, quenched quickly and the spectrum was recorded at 298 K in the wavelength region 200–900 nm. Solution (a), containing $Co(OAc)_2 \cdot 4H_2O$/NaBr/HOAc/H_2O/air, showed a broad asymmetric band, with a band maximum at 520 nm and two shoulders at 470 and 450 nm. These bands, corresponding to d–d transitions, are typical of an octahedrally coordinated Co(II)-acetato complex

[12,25]. The solution on contact with O_2 (air) showed marked changes in the electronic spectrum. Representative spectra for $Co(OAc)_2 \cdot 4H_2O/NaBr/HOAc/H_2O$/air solutions are shown in Fig. 1(a). The optical density of the band, at 520 nm, increased gradually on interaction with oxygen and a new, weak band, characteristic of the Co(III)-acetato complex, appeared at 630 nm [12]. The enhanced optical density of the band at 520 nm suggests the formation of yet another Co(II) complex, probably Co(OAc)Br, having a symmetry lower than that of $Co(OAc)_2 \cdot 4H_2O$. The lower symmetry of Co(OAc)Br admixes the molecular orbitals and allows the d–d transitions. As a consequence, the intensity of the d–d transitions for Co(OAc)Br are higher than that of $Co(OAc)_2 \cdot 4H_2O$ (Fig. 1(a)).

Interestingly, solution (b), containing the substrate PX, (Fig. 1(b)) did not show the above spectral changes even after several hours, on interaction with air. This difference in the spectral behaviour in the presence of PX, suggests that Co(III)-acetato and Co(OAc)Br species, formed during the air/dioxygen oxidation, are highly reactive towards the substrate, PX and, hence, have very short lifetimes.

To elucidate the role of $Mn(OAc)_2 \cdot 4H_2O$, spectral studies were carried out in the system $Co(OAc)_2 \cdot 4H_2O/Mn(OAc)_2 \cdot 4H_2O/NaBr/HOAc/H_2O/PX$ (solution (c)). $Mn(OAc)_2 \cdot 4H_2O$ does not exhibit any band due to the metal-centered, d–d transitions. However, on interaction with O_2, new features characteristic of an oxo-bridged Mn(III) cluster complex [30–32] appeared at 460 and 350 nm, in addition to the band at 520 nm. The latter is characteristic of $Co(OAc)_2 \cdot 4H_2O$. The band at 460 nm corresponds to the d–d transition while that at 350 nm is attributed to the ligand-to-metal charge transfer (LMCT) transition [30–32]. Co(III)-acetato complexes (630 nm), could not be detected in the spectrum for $Co(OAc)_2 \cdot 4H_2O/Mn(OAc)_2 \cdot 4H_2O/NaBr/HOAc/H_2O/PX$/air. The intensity of the bands at 460 and 350 nm, due to Mn(III) cluster complex increased during the course of the reaction. Typical spectra for solution (c) are shown in Fig. 1(c).

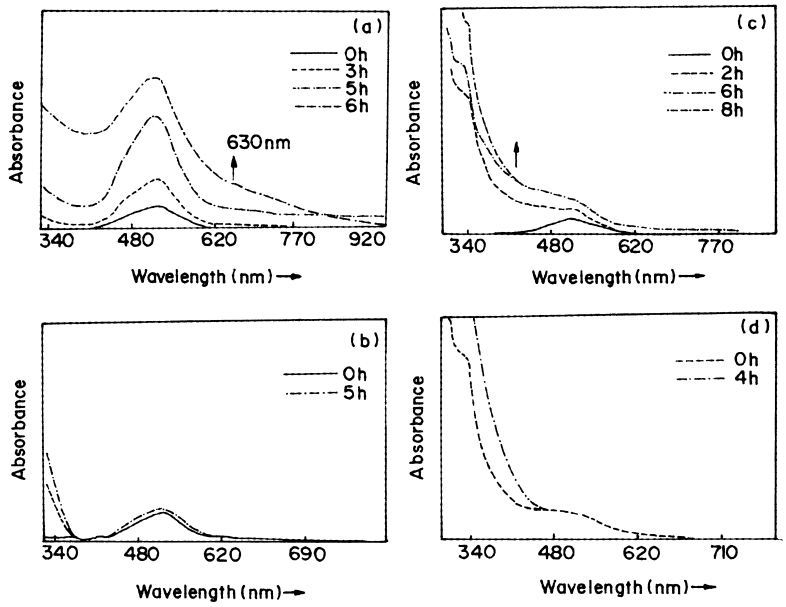

Fig. 1. Electronic spectra as a function of time: (a) $Co(OAc)_2 \cdot 4H_2O$ (1.03 mmol)/NaBr (1.35 mmol)/HOAc (587 mmol)/H_2O (311 mmol)/air; (b) $Co(OAc)_2 \cdot 4H_2O$ (1.03 mmol)/NaBr (1.35 mmol)/HOAc (587 mmol)/H_2O (311 mmol)/PX (44.3 mmol)/air; (c) $Co(OAc)_2 \cdot 4H_2O$ (1.03 mmol)/$Mn(OAc)_2 \cdot 4H_2O$ (0.35 mmol)/NaBr (1.35 mmol)/HOAc (587 mmol)/H_2O (311 mmol)/PX (44.3 mmol)/air; (d) $Co(OAc)_2 \cdot 4H_2O$ (1.03 mmol)/$Mn(OAc)_2 \cdot 4H_2O$ (0.35 mmol)/NaBr (1.35 mmol)/HOAc (587 mmol)/H_2O (311 mmol)/PX (44.3 mmol)/H_2O_2.

The Mn(III) oxo-cluster complexes are also seen when H_2O_2 is substituted for O_2 (solution (d), (Fig. 1(d))). In oxidation with air the reaction had to be carried out for a minimum period of 3–5 h before Mn(III) cluster complexes could be detected. They are, however, formed instantaneously on the addition of H_2O_2 (compare Fig. 1(d) with (c)). In the absence of cobalt, solutions containing only manganese, like solution (e), $Mn(OAc)_2 \cdot 4H_2O/NaBr/HOAc/H_2O/PX$/air, did not reveal the formation of Mn(III) cluster complexes. When cobalt(II) is present, it is probably oxidized initially to a Co(III) complex which promotes the oxidation of Mn(II) to a Mn(III) cluster complex. When H_2O_2 was used as the oxidant both Co(II) and Mn(II), are oxidized simultaneously to their corresponding +3 oxidation states.

3.2. EPR spectroscopy

EPR investigations were carried out on the following solutions.

(i) $Co(OAc)_2 \cdot 4H_2O$ (1.03 mmol)/NaBr (1.35 mmol)/HOAc (587 mmol)/H_2O (311 mmol); ($Co:Br^- = 3:4$).

(ii) $Co(OAc)_2 \cdot 4H_2O$ (1.03 mmol)/NaBr (1.35 mmol)/HOAc (587 mmol)/H_2O (311 mmol)/pyridine (25 mmol)/H_2O_2; ($Co:Br^- = 3:4$).

(iii) $Co(OAc)_2 \cdot 4H_2O$ (1.03 mmol)/$Mn(OAc)_2 \cdot 4H_2O$ (0.35 mmol)/NaBr (1.35 mmol)/HOAc (587 mmol)/H_2O (311 mmol)/PX (44.3 mmol)/air; ($Co:Mn:Br^- = 3:1:4$).

(iv) $Co(OAc)_2 \cdot 4H_2O$ (0.35 mmol)/$Mn(OAc)_2 \cdot 4H_2O$ (1.03 mmol)/NaBr (1.35 mmol)/HOAc (587 mmol)/H_2O (311 mmol)/PX (44.3 mmol)/air; ($Co:Mn:Br^- = 1:3:4$).

(v) $Mn(OAc)_2 \cdot 4H_2O$ (1.03 mmol)/NaBr (1.35 mmol)/HOAc (587 mmol)/H_2O (311 mmol)/PX (44.3 mmol)/air ($Mn:Br^- = 3:4$).

(vi) $Co(OAc)_2 \cdot 4H_2O$ (1.03 mmol)/$Mn(OAc)_2 \cdot 4H_2O$ (0.35 mmol)/$Zr(OH)_4$ (0.1 mmol)/NaBr (1.35 mmol)/HOAc (587 mmol)/H_2O (311 mmol)/PX (44.3 mmol)/air; ($Co:Mn:Zr:Br^- = 3:1:0.3:4$).

Solution (i) did not show any EPR signal at 298 K. The spectrum at 77 K (Fig. 2, curve (a)) was a broad asymmetric signal with a width of about 5500 G. The broad feature is due to the short electron spin lattice relaxation time of Co(II) ions in HOAc. However, on addition of pyridine, the purple coloured solution (ii) showed a spectrum characterized by an axially symmetric g tensor ($g_\perp = 7.02$ and $g\| = 1.11$) (Fig. 2, curve (b)). The signals are attributed to a $Co(OAc)_2(pyridine)_4$ complex [33]. Upon interacting with H_2O_2, the overall spectral intensity decreased by about 30% and the signal was further broadened (Fig. 2, curve (c)). The reduction in spectral intensity reveals the formation of Co(III)-acetato/oxo-bridged Co(III) cluster complexes. Oxo-bridged cluster complexes of the composition $[(pyridine)_3Co_3O(OAc)_6]^+$ and $[(pyridine)_3Co_3O(OAc)_5(OH)]^+$ have been isolated and structurally characterized by Sumner and Steinmetz [23,24] and Beattie et al. [34].

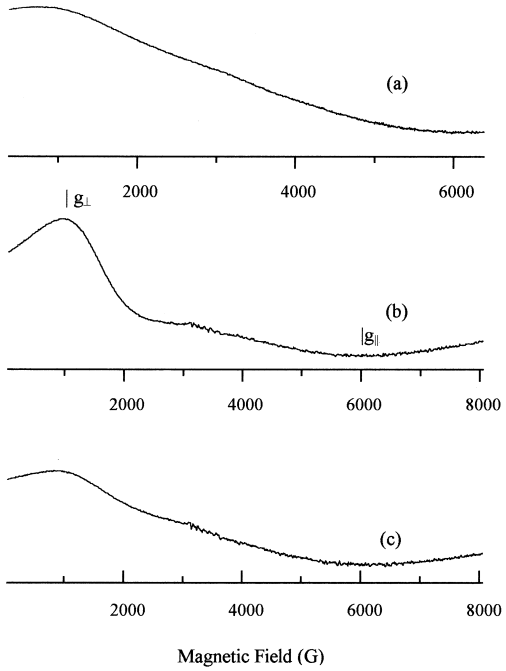

Fig. 2. X-band EPR spectra at 77 K: (a) $Co(OAc)_2 \cdot 4H_2O$ (1.03 mmol)/NaBr (1.35 mmol)/HOAc (587 mmol)/H_2O (311 mmol); (b) $Co(OAc)_2 \cdot 4H_2O$ (1.03 mmol)/NaBr (1.35 mmol)/HOAc (587 mmol)/H_2O (311 mmol)/pyridine (25 mmol); (c) $Co(OAc)_2 \cdot 4H_2O$ (1.03 mmol)/NaBr (1.35 mmol)/HOAc (587 mmol)/H_2O (311 mmol)/pyridine (25 mmol)/H_2O_2.

Narrow signals due to Mn(II) dominated those of high spin Co(II) in solutions (iii), (iv) and (vi). Solution (iii) showed a resolved, sextet line, hyperfine pattern due to Mn(II) at 298 K (Fig. 3(a)). The spin Hamiltonian parameters, ($g_{iso} = 2.0012$ and $A_{iso} = 93.8$ G) indicate an octahedral geometry for the Mn(II) ion [35]. On passing air through the reaction mixture, for 3 h, the overall intensity of the spectrum decreased by about 35% (Fig. 3(b)) suggesting oxidation of a part of Mn(II) to Mn(III) ions. The spectra at 77 K consist of an unresolved central zero-field signal (m_s: $-1/2 \leftrightarrow +1/2$) typical for weakly interacting Mn(II) ions in linear trimeric $Mn(OAc)_2 \cdot 4H_2O$ complex (Fig. 3(c) and (d)). At 77 K, interaction with air showed improved resolution of manganese hyperfine features (Fig. 3(d)).

Solution (iv) containing 0.35 mmol of cobalt and 1.03 mmol of manganese salts showed similar spectral behaviour as that of solution (iii) (Fig. 4(a)). The overall intensity of the sextet pattern, at 298 K, decreased during air oxidation (Fig. 4(a)–(c)). The outermost hyperfine signals became more intense than the inner ones. The linewidth increases from 45 to 72 G on interaction with air (Table 1). Moreover, changes in spin Hamiltonian parameters ($g_{iso} = 2.0005$ and $A_{iso} = 94.6$ G) were also noticed during the course of the reaction. Addition of pyridine to the reaction mixture showed marked changes in the overall spectral intensity as well as the intensity of outer and innermost hyperfine signals (compare Fig. 4(b) with (d)). The spectrum could be fitted to the presence of two types of signals overlapping with each other, one with a sextet pattern corresponding to monomeric Mn(II) ions in $Mn(OAc)_2(pyridine)_4$ complex ($g_{iso} = 2.000$ and $A_{iso} = 92$ G) [35] and the other, a broad signal at $g_{iso} = 1.992$, due to the Mn cluster complex $Mn_3O(OAc)_6(pyridine)_3$ [30,32]. The spectra for solution (iv), recorded at 77 K, are

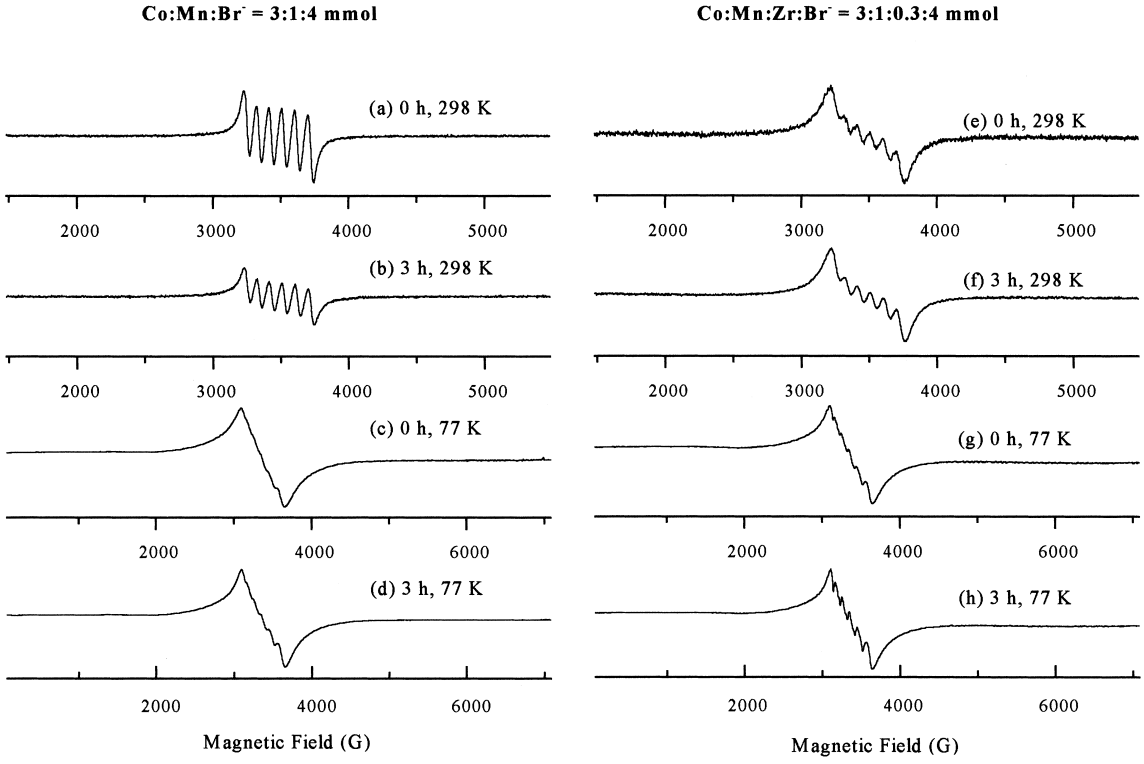

Fig. 3. EPR spectra of $Co(OAc)_2 \cdot 4H_2O$ (1.03 mmol)/$Mn(OAc)_2 \cdot 4H_2O$ (0.35 mmol)/NaBr (1.35 mmol)/HOAc (587 mmol)/H_2O (311 mmol)/PX (44.3 mmol)/air at (a) 0 h, 298 K; (b) 3 h, 298 K; (c) 0 h, 77 K; (d) 3 h, 77 K, respectively, and $Co(OAc)_2 \cdot 4H_2O$ (1.03 mmol)/$Mn(OAc)_2 \cdot 4H_2O$ (0.35 mmol)/$Zr(OH)_4$ (0.1 mmol)/NaBr (1.35 mmol)/HOAc (587 mmol)/H_2O (311 mmol)/PX (44.3 mmol)/air at (e) 0 h, 298 K; (f) 3 h, 298 K; (g) 0 h, 77 K; (h) 3 h, 77 K, respectively.

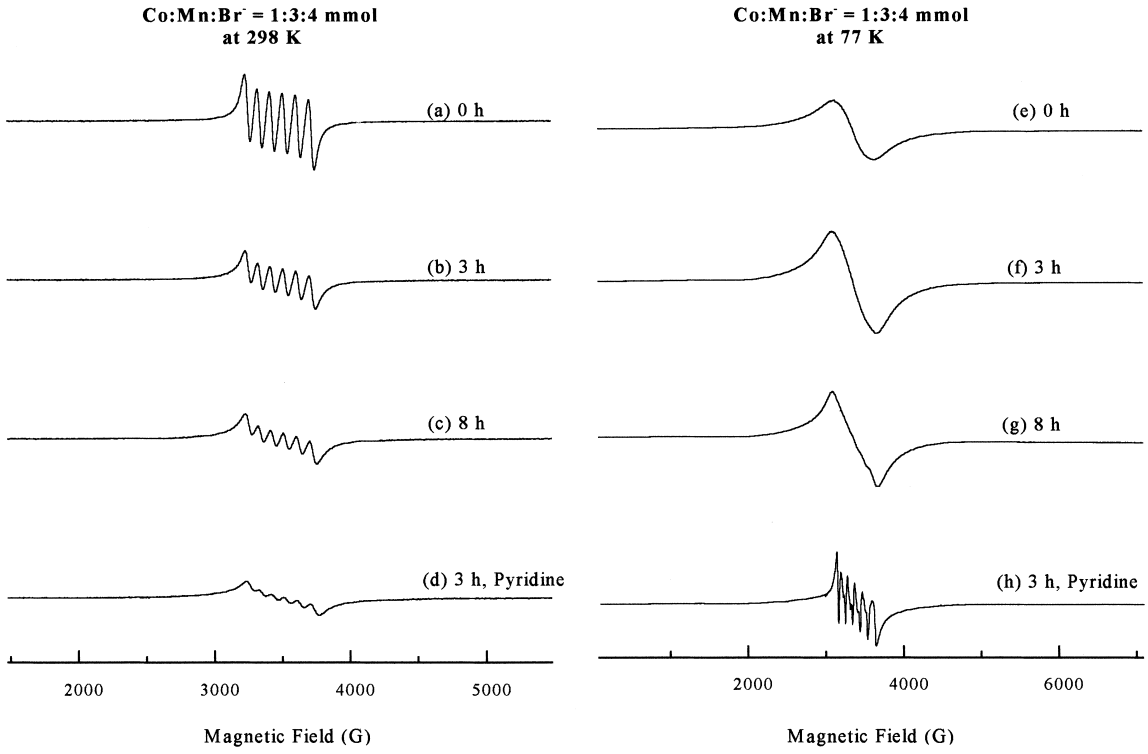

Fig. 4. EPR spectra, as a function of time, of $Co(OAc)_2 \cdot 4H_2O$ (0.35 mmol)/$Mn(OAc)_2 \cdot 4H_2O$ (1.03 mmol)/NaBr (1.35 mmol)/HOAc (587 mmol)/H_2O (311 mmol)/PX (44.3 mmol)/air: Curves (a)–(d) refer to (a) 0 h; (b) 3 h; (c) 8 h and (d) 3 h with pyridine at 298 K and curves (e)–(h) refer to (e) 0 h; (f) 3 h; (g) 8 h and (h) 3 h with pyridine at 77 K, respectively.

depicted in Fig. 4(e)–(h). Addition of pyridine enhanced the formation of oxo-bridged Mn cluster complexes. The resolved Mn hyperfine features at 77 K in pyridine-containing solutions are typical of non-interacting Mn(II) ions (Fig. 4(h)); the Mn(III) cluster complex is EPR silent at 77 K due to intermolecular antiferromagnetic interactions. The broad signal for the cluster complex, at 298 K, perhaps, arises due to population of low lying paramagnetic excited triplet states ($S' = 1$) [30].

Solution (vi) is similar to solution (iii) except that the former contains a small quantity of $Zr(OH)_4$ (0.1 mmol) as an additive. Their spectra are, however, markedly different (compare Fig. 3(e)–(h) with Fig. 3(a)–(d), respectively). The manganese hyperfine pattern is well resolved in solution (iii) without Zr(IV) ion, while solution (vi) containing Zr(IV) additive showed only a partially resolved hyperfine pattern (similar to that observed for (iii) and (iv) after interacting with air for several hours; see Fig. 4(c) and (d) for comparison). Surprisingly, unlike solutions (iii) and (iv), the solution containing Zr(IV) ions showed no change in overall spectral intensity even after 8 h of interaction with air (see Fig. 3(e) and (f)). The spectra at 77 K (Fig. 3(g) and (h)) resemble those of solution (iii) at 77 K (Fig. 3(c) and (d)). However, they are significantly different from those of solution (iv) (Fig. 4(e) and (g)). This difference in the spectral behaviour is due to the following reasons: the presence of Zr(IV) enhances the oxidations of Co(II) to Co(III) and subsequently, Mn(II) to Mn(III). This enhancement enables the formation of Mn(III) cluster complexes. These cluster complexes are different in composition in solutions (iii), (iv) and (vi). From the spectral differences, we conclude that solution (iv) contains homonuclear $Mn_3(O)(OAc)_x$ type clusters (characterized by $g_{iso} = 2.0005$ and spectral width $= 525$ G) as the major species with a minor component being $CoMn_2(O)(OAc)_x$ clusters; Solutions (iii) and (vi) contain the heteronuclear clusters of the type $Co_2Mn(O)(OAc)_x$ as a predominant species and $Co_3(O)(OAc)_x$ and

Table 1
EPR spin Hamiltonian parameters of Mn in Co/Mn/Zr/Br system at 298 K

Catalyst[a]	Conditions[b]	g_{iso}	A_{Mn} (G)	ΔH_{pp} (G)	Spectral width (G)	Remarks
Co(1.03) + Mn(0.35) + Br(1.35)	Without O_2, 0 h	2.0012	93.8	45	511	Resolved sextet
	With O_2, 3 h	2.0012	92.0	45	516	Resolved sextet
	With O_2, 3 h + pyridine	1.9960	92.0	85	526	Interacting Mn clusters
Co(1.03) + Mn(0.35) + Br(1.35)	Without O_2, 0 h	2.0014	93.8	45	511	Resolved sextet
	With O_2, 3 h	2.0012	93.6	60	516	Small amounts of interacting Mn clusters
	With O_2, 8 h	2.0005	94.6	72	525	Interacting Mn clusters
	With O_2,8 h + pyridine	1.9920	92.0	85	530	High amounts of interacting Mn clusters
Co(1.03) + Mn(0.35) + Zr(0.1) + Br(1.35)	Without O_2, 0 h	2.0015	94.6	95	546	Interacting Mn clusters
	With O_2, 3 h	2.0000	94.6	95	547	Interacting Mn clusters
	With O_2, 5 h	1.9980	94.6	95	547	High amounts of interacting Mn clusters
Co(1.03) + Mn(0.35) + Br(2.03)	Without O_2, 0 h	2.0000	93.0	70	548	Interacting Mn clusters
	With O_2, 1–7 h	2.0000	92.0	75	544	Interacting Mn clusters
Co(1.35) + Mn(0.35) + Br(6.09)	Without O_2, 0 h	2.0025	93.8	55	527	Resolved sextet
	With O_2, 1–5 h	2.0025	93.8	55	527	Resolved sextet
Co(1.35) + Mn(0.35) + Br(10.2)	Without O_2, 0 h	2.0025	93.8	58	528	Resolved sextet
	With O_2, 1–5 h	2.0025	93.8	58	528	Resolved sextet

[a] Values in the parentheses refer to the number of mmol of catalyst in HOAc.
[b] Air was used as the source of O_2.

$CoMn_2(O)(OAc)_x$ as minor species (characterized by $g_{iso} = 2.0012$ and spectral width = 516 G for solution (iii) and $g_{iso} = 1.998$ and spectral width = 547 G for solution (vi)).

Solution (v) containing $Mn(OAc)_2 \cdot 4H_2O$ (1.03 mmol)/NaBr (1.35 mmol)/HOAc (587 mmol)/H_2O (311 mmol)/PX (44.3 mmol) shows resolved hyperfine pattern as observed for solution (iv) (Fig. 4(a)). The changes are only marginal on interaction with air. This result is in agreement with the electronic spectral studies. Both the spectral techniques, suggest that the oxidation of Mn(II) to Mn(III) species is difficult in the absence of cobalt or zirconium salts. Table 1 gives a summary of the EPR spin Hamiltonian parameters at 298 K.

EPR studies were also carried out on the following reaction mixtures (containing excess Br^-) to investigate the effect of bromide ion on the speciation.

(vii) $Co(OAc)_2 \cdot 4H_2O$ (1.03 mmol)/$Mn(OAc)_2 \cdot 4H_2O$ (0.35 mmol)/NaBr (2.03 mmol)/HOAc (587 mmol)/H_2O (311 mmol)/PX (44.3 mmol)/air; (Co:Mn:Br^- = 3:1:6).

(viii) $Co(OAc)_2 \cdot 4H_2O$ (1.03 mmol)/$Mn(OAc)_2 \cdot 4H_2O$ (0.35 mmol)/NaBr (6.09 mmol)/HOAc (587 mmol)/H_2O (311 mmol)/PX (44.3 mmol)/air; (Co:Mn:Br^- = 3:1:18).

(ix) $Co(OAc)_2 \cdot 4H_2O$ (1.03 mmol)/$Mn(OAc)_2 \cdot 4H_2O$ (0.35 mmol)/NaBr (10.2 mmol)/HOAc (587 mmol)/H_2O (311 mmol)/PX (44.3 mmol)/air; (Co:Mn:Br^- = 3:1:30).

Fig. 5 depicts the EPR spectra at 298 K of the reaction mixtures containing different concentrations of NaBr before reacting with O_2 (air, 0 h). The type of Mn species varies with Br^- ion concentration. The spin Hamiltonian parameters (Table 1), especially g_{iso}, ΔH_{pp}, and spectral width are different. Interestingly, the spectrum for solution (vii) (Co:Mn:Br molar ratio = 3:1:6, Fig. 5(b)) is similar to the oxygenated solutions (iii) and (iv) with low bromide ion contents (e.g. Co:Mn:Br = 3:1:4 mmol; Fig. 3(b)). The spectra are also similar to that of zirconium-containing solution (vi) (Fig. 3(f)) and reveal the presence of highly interacting Mn cluster species ($g_{iso} = 2.000$ and spectral width = 544 G). The spectrum for the solution containing lower amounts of Br^- ion (Fig. 5(a)) corresponds to that of

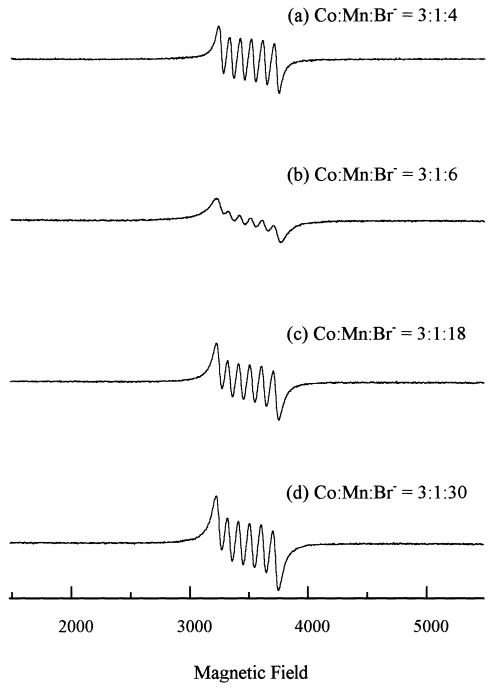

Fig. 5. Influence of Br^- on the EPR spectra of $Co(OAc)_2 \cdot 4H_2O$ (1.03 mmol)/$Mn(OAc)_2 \cdot 4H_2O$ (0.35 mmol)/NaBr (x mmol)/HOAc (587 mmol)/H_2O (311 mmol)/PX (44.3 mmol)/air: x = 1.35, 2.03, 6.1 and 10.2 for curves (a)–(d), respectively.

$Mn(OAc)_2 \cdot 4H_2O$ in HOAc. On the other hand, the spectra for solutions having higher amounts of Br^- ion (Fig. 5(c) and (d)) indicate the presence of only weakly interacting Mn(II) ions. Thus, the linear trimeric structure of $Mn(OAc)_2 \cdot 4H_2O$ is converted to oligomeric species in the presence of cobalt and Br^- ions. At a Co:Mn:Br ratio of 3:1:6, for example, a majority of the Co and Mn are present as cluster complexes, $Co_2Mn(O)(OAc)_x$ and $CoMn_2(O)(OAc)_x$. At higher Br^- ion concentrations, a linear acetato bridged chain structure, with weakly interacting Mn ions, is formed.

Typical spectra for solution (vii) are shown in Fig. 6. No major changes were noticed in the EPR spectrum during the course of the reaction. The behaviour is similar to that of solutions (vi) containing zirconium as an additive. In other words, the induction periods to generate the cluster complexes are reduced considerably by the addition of excess

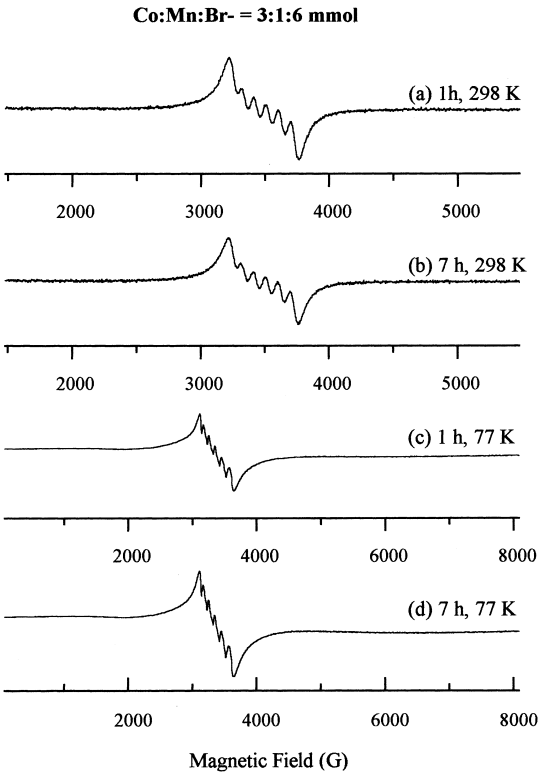

Fig. 6. EPR spectra of $Co(OAc)_2 \cdot 4H_2O$ (1.03 mmol)/$Mn(OAc)_2 \cdot 4H_2O$ (0.35 mmol)/NaBr (2.03 mmol)/HOAc (587 mmol)/H_2O (311 mmol)/PX (44.3 mmol)/air; (a) 1 h, 298 K; (b) 7 h, 298 K; (c) 1 h, 77 K; (d) 7 h, 77 K, respectively.

Br^- or zirconium ions. The optimum proportion of the constituents to generate the cluster species was found to be Co:Mn:Br = 3:1:6 mmol.

$Co(OAc)_2 \cdot 4H_2O$ and $Ni(OAc)_2 \cdot 4H_2O$ have an isomorphous structure in solid state [36] and form one-dimensional chains (Scheme 1(A)) with acetato ligands bridging adjacent Co or Ni atoms [36]. $Mn(OAc)_2 \cdot 4H_2O$, on the other hand, is trimeric and forms a two dimensional layered network, with adjacent trimer units interconnected through bridging acetato groups (Scheme 1(B)) [37]. The symmetry around the metal is octahedral. The cobalt and nickel acetate complexes are present as monomers in acetic acid solution while $Mn(OAc)_2 \cdot 4H_2O$ is present as a trimer (as may be inferred from a comparison with the EPR spectra of frozen solutions). Monomeric non-interacting Mn(II) ions in solution show an EPR spectrum at 298 K consisting of six well resolved equally intense hyperfine lines due to the interaction of Mn(II) nuclear spin ($S = 5/2$, $I = 5/2$). Frozen solutions of Mn(II), at 77 K, exhibit six major lines due to the zero-field transitions of m_S: $|-1/2> \leftrightarrow |+1/2>$, while the other sets of transitions corresponding to m_S: $|\pm 5/2> \leftrightarrow |\pm 3/2>$ and $|\pm 3/2> \leftrightarrow |\pm 1/2>$ are usually not resolved due to large zero-field anisotropy; They contribute only to the background upon which the six major hyperfine signals are superimposed. Further, two small forbidden transitions due to $\Delta m_I = \pm 1$ appear between the adjacent hyperfine features. In the case of interacting Mn(II) ions, the nature of the spectrum depends upon the magnitude of the exchange interaction (J). If the exchange coupling constant is small, the linewidths (ΔH_{pp}) will be larger and the hyperfine features are only partially resolved. The intensities of the outmost and inner hyperfine signals will be different. In frozen solutions, at 77 K, in addition to the exchange interactions, the dipole–dipole interactions also con-

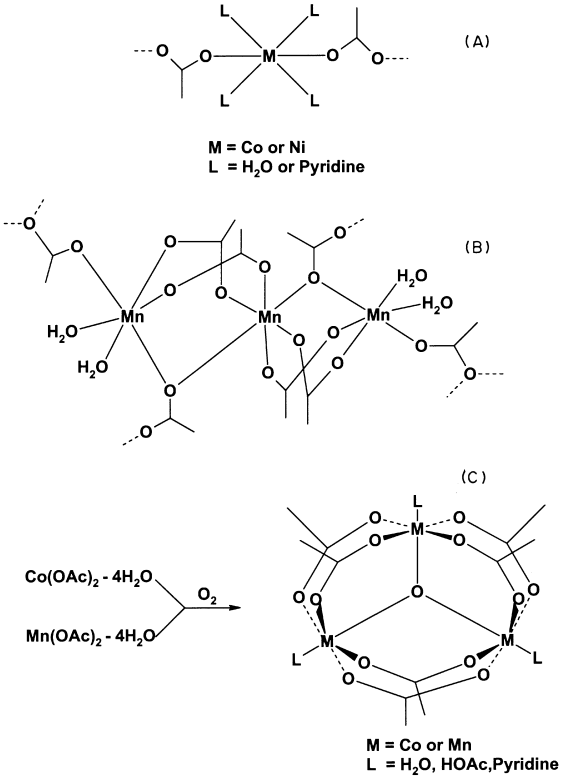

Scheme 1.

tribute and as a consequence of this the sextet hyperfine feature from the zero-field transition m_S: $|-1/2> \leftrightarrow |+1/2>$ will not be resolved. The EPR spectra of Co/Mn/Br (before reacting with O_2) indeed belong to this category. If the exchange coupling constant (J) is high, only an exchange narrowed line is observed in place of the sextet hyperfine pattern. In fact, the cluster complexes formed during the course of the reaction belong to this category. It is pertinent to note that the oxo-bridged $Mn_3O(OAc)_6(pyridine)_3$ cluster complex (Scheme 1(C)) has an exchange coupling constant of $10.2\,cm^{-1}$ while $Mn(OAc)_2 \cdot 4H_2O$ has a value of $0.5\,cm^{-1}$. The difference between the spectral pattern before and after reacting with O_2, especially for solutions (iii) and (iv) are due to formation of the oxo-bridged Mn cluster complexes. The higher resolution in the hyperfine pattern (Fig. 3(d) and (h))

Table 2
Catalytic data for the oxidation of *p*-xylene[a]

Run	Catalyst composition[b] (mmol)	Time (h)	Conversion (wt.%)	TOF[c]	Product distribution (wt.%)[d]				
					A	B	C	D	E
1	Co(1.03)	8.0	28.2	1.5	2.6	91.5	5.9		
2	Co(1.03) + Mn(0.35)	16.0	98.0	2.0	0.4	18.2	76.4	2.0	3.0
2A	Co(1.03) + Mn(0.35)	8.0	99.7	3.9	5.7	46.6	18.2	13.0	16.5
2B	Co(1.03) + Mn(0.35)	7.0	97.3	4.5	2.4	34.0	38.4	15.2	10.0
2C	Co(1.03) + Mn(0.35)	6.3	99.5	5.1	2.8	36.0	36.6	17.4	7.0
2D	Co(1.03) + Mn(0.35)	4.5	99.2	7.0	3.5	44.5	27.8	17.0	7.2
3	Co(0.7) + Mn(0.7)	16.0	81.0	1.1	5.5	19.4	71.5	3.0	0.3
4	Co(0.35) + Mn(1.03)	16.0	31.6	0.6	1.6	94.6	3.8		
5	Mn(1.03)	8.0	12.0	0.6	1.5	96.4	2.1		
Effect of zirconium									
6	Co(1.03) + Mn(0.35) + Zr(0.1)	7.5	92.0	3.7	1.7	33.3	36.0	21.0	8.0
6A	Co(1.03) + Mn(0.35) + Zr(0.1)	5.9	96.0	5.8	7.6	60.0	8.5	12.5	11.4
7	Co(1.03) + Mn(0.35) + Zr(0.1)	6.5	93.4	3.8	3.8	33.7	53.8	7.4	1.3
8	Co(1.03) + Mn(0.35) + Zr(0.6)	7.5	86.8	3.0	3.4	24.1	64.6	6.0	1.9
9	Co(1.03) + Mn(0.35) + Zr(0.05)	10.0	81.6	2.5	2.2	33.8	56.3	6.5	1.2
10	Co(0.35) + Mn(1.03) + Zr(0.1)	6.5	38.0	1.8	6.2	93.6	0.2		
11	Co(0.35) + Mn(1.03) + Zr(0.1)	10.0	55.0	1.6	8.1	91.0	0.9		
12	Co(0.35) + Mn(1.03) + Zr(0.1)	16.0	87.8	1.7	2.8	30.2	63.5	1.5	2.0
13	Co(0.35) + Zr(1.03)	5.0	16.0	0.7	6.2	90.3	3.5		
Effect of cerium									
14	Co(1.03) + Mn(0.35) + Ce(0.1)	10.5	51.5	1.5	11.6	80.4	8.0		
14A	Co(1.03) + Mn(0.35) + Ce(0.1)	8.5	98.5	3.5	8.6	51.7	29.7	7.0	3.0
15	Co(0.35) + Mn(1.03) + Ce(0.1)	10.5	41.0	1.2	10.7	88.6	0.7		
16	Co(0.35) + Ce(1.35)	5.0	15.5	1.5	51.8	42.7	5.5		
Effect of nickel									
17	Ni(1.03) + Mn(0.35)	16.0	17.0	0.3	17.3	82.7			
18	Ni(0.7) + Mn(0.7)	16.0	24.0	0.3	19.3	66.8	13.9		
19	Ni(0.35) + Mn(1.35)	16.0	13.2	0.3	6.2	90.9	2.9		
20	Ni(0.35) + Mn(1.35) + Zr(0.1)	16.0	67.1	1.2	15.2	58.4	26.0	0.2	0.2

[a] Reaction conditions: medium-*p*-xylene (44.3 mmol) + NaBr (1.35 mmol) + H_2O (311 mmol) + HOAc (587 mmol); air, atmospheric pressure; temperature, 363 K.

[b] The sources of Co, Mn, Ni, Zr and Ce are $Co(OAc)_2 \cdot 4H_2O$, $Mn(OAc)_2 \cdot 4H_2O$, $Ni(OAc)_2 \cdot 4H_2O$, $Zr(OH)_4$ and $Ce(NO_3)_3 \cdot 6H_2O$, respectively. Values in the parentheses refer to the number of mmol of catalyst. In Runs 2A, 6A and 14A, 2.03 mmol of NaBr was used. In Runs 2B, 2C and 2D, 3.51, 6.09 and 10.2 mmol of NaBr were used, respectively.

[c] Turnover frequency (TOF) = mole of *p*-xylene converted per mole of metal catalyst per hour.

[d] A = *p*-tolyl alcohol, B = *p*-tolyl aldehyde, C = *p*-toluic acid, D = 4-carboxybenzaldehyde and E = terephthalic acid.

after interacting with O_2 is an indication of formation of monomeric Mn(II) ions. The structures of the various species are shown in Scheme 1.

3.3. Oxidation of p-xylene

The conversion and product distribution in the oxidation of PX over Co/Mn, Co/Mn/Zr, Co/Mn/Ce and Ni/Mn/Zr catalyst systems are presented in Table 2. Under our mild conditions (363 K), *p*-tolyl alcohol (A), *p*-tolyl aldehyde (B), *p*-toluic acid (C), 4-carboxybenzaldehyde (D) and terephthalic acid (E) are the main products in the oxidation of PX. Co or Mn acetates alone gave low conversions and *p*-tolyl aldehyde was the major oxidation product (Runs 1 and 5, Table 2). A combination of Co and Mn salts resulted in much higher conversions. The catalyst with Co to Mn mmol ratio of 3:1 showed the highest conversion; *p*-toluic acid was the major oxidation product and 4-CBA and TA were the minor oxidation products. When the catalyst contained more Mn than Co (Run 4), *p*-tolyl aldehyde was the major product. A novel and interesting finding is the significant enhancement in catalytic activity and yield of TA formed at higher Br^- concentrations (compare Run 2 with Runs 2A–2D). The values of the turnover frequencies for PX conversion (TOF) have increased by three and half times with increasing Br^- ion concentrations. Similar conversions were attained more quickly.

Addition of Zr enhanced the conversion and the product contained higher amounts of 4-CBA and TA (Runs 6–13). PX conversion is, however, suppressed at high Zr concentrations (compare Runs 7 and 8). The promotional effect of Br^- is also observed (compare Runs 6 and 6A).

Conversions with Ce were lower (Runs 14–16). Ce-containing catalysts showed higher selectivity for *p*-tolyl aldehyde. A novel finding is that the Co/Ce catalyst, in the absence of Mn, was the only catalyst in our investigation to exhibit a high selectivity for *p*-tolyl alcohol (Run 16), a speciality chemical. At similar or even lower conversion levels other catalyst systems like Co/Zr (Run 13), Ni/Mn (Run 17) and Mn (Run 5) exhibited much lower selectivities for *p*-tolyl alcohol. Again, Br^- enhances significantly both the TOF and yield of TA (compare Runs 14 and 14A).

The activity of Ni/Mn catalysts is illustrated in Runs 17–19. The conversions in the absence of cobalt, and even after 16 h of reaction time, are very low. *p*-Tolyl aldehyde was the major product. Addition of Zr to Ni/Mn catalyst (Run 20) enhances the activity significantly. Although *p*-tolyl aldehyde was still the major product, small quantities of 4-CBA and TA were also formed. The high conversion levels and the presence of 4-CBA and TA even in the absence of cobalt are surprising novel findings.

Partenheimer reported [12] that the oxidation of acetic acid to CO_2 in the system cobalt-O_2-HOAc was promoted by Co(III). In our studies, loss of HOAc was not observed at 363 K with the Co/Mn, Ni/Mn or Co/Mn/Ce catalyst systems even at near-complete conversion of PX (Run 2). This may perhaps be due to the fast reduction of Co(III) to Co(II) by Mn(II). Co(III) ions are, hence, not available for the oxidation of HOAc. We observed the loss in HOAc at this temperature (about 10 wt.%) only when Zr was used. An interesting observation is that the oxidation of HOAc to CO and CO_2 depended more on the catalyst/promoter system and temperature of oxidation rather than the PX conversion level. Hence, it is possible, at least in principle, to reduce the HOAc loss by choice of a catalyst and solvent system which can oxidize *p*-tolyl aldehyde, *p*-toluic acid and 4-CBA to TA at lower temperatures.

The EPR spectra for the solutions with different Br^- ion concentrations at 298 K and at reaction time of 3 h were deconvoluted. The ratio of the intensity of cluster complexes ($Co_2Mn(O)(OAc)_x$ and $CoMn_2(O)(OAc)_x$) to $Mn(OAc)_2$ increases with increasing $[Br^-]/([Co]+[Mn])$ ratio, reaching a maximum for Co:Mn:Br^- = 3:1:6 mmol and then decreases (Fig. 7(a)). The catalytic activity (TOF), on the other hand, increases continuously with Br^- concentration (Fig. 7(b)). The amounts of 4-CBA and TA formed during the oxidation reaction (Fig. 7(c)) follow changes in the ratio of the intensity of cluster complexes to $Mn(OAc)_2$. Cluster complexes (like $Co_2Mn(O)(OAc)_x$ and $CoMn_2(O)(OAc)_x$) probably play an important role in the further oxidation of *p*-toluic acid to 4-carboxybenzaldehyde and terephthalic acid.

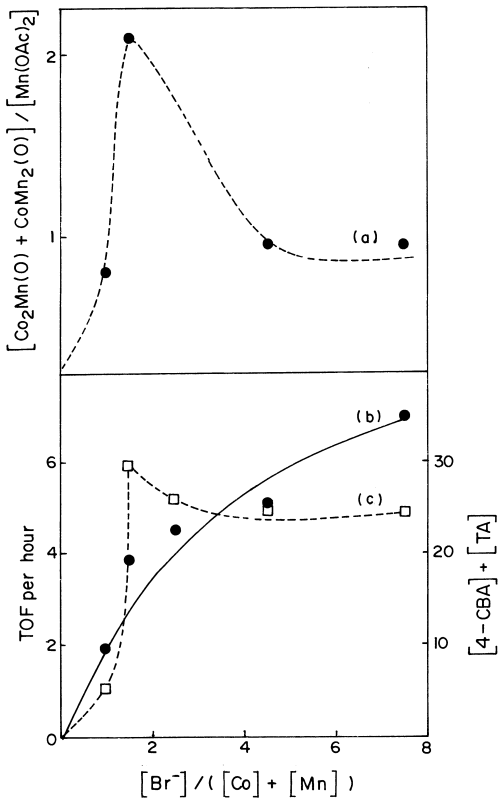

Fig. 7. Variation of the intensity ratio of cluster complexes $[Co_2Mn(O)+CoMn_2(O)]$ to $Mn(OAc)_2$ species (curve (a)), TOF per hour (curve (b) and ([4-CBA]+[TA]) (curve (c)) vs. $[Br^-]/([Co]+[Mn])$. The signal intensities of cluster and $Mn(OAc)_2$ complexes were estimated from the EPR spectra (298 K) of the solutions recorded at a reaction time of 3 h.

The catalytic activity studies in the oxidation of PX reveal the following: (1) catalytic activity is synergistically enhanced when both Co and Mn are present and Co is in excess, (2) Zr in small quantities enhances the PX conversion and selectivity for 4-CBA and TA significantly. The combination of Co/Mn/Zr with mmol ratio of 7:3 $\leq$ was found to give the highest conversion of PX and yield of TA among the systems studied here, (3) while Ce-containing catalysts were less active than those containing Zr, their selectivity for *p*-tolyl alcohol was much higher, (4) While Ni/Mn catalysts were also much less active than Co/Mn samples, their activity could be enhanced significantly by Zr, (5) high concentrations of bromide ions enhanced, significantly, both PX conversions and yield of TA, and (6) there is a correlation between the yield of 4-CBA + TA and the concentration of the Co/Mn cluster complexes.

3.4. Role of cobalt and manganese cluster complexes in the oxidation of p-xylene

The aerial oxidation of PX by the Co/Mn/Br catalyst system follows a free radical chain mechanism [3]. Co(III) is the radical initiating species formed from $Co(OAc)_2$ either by reaction with O_2 or with adventitious peroxides present in acetic acid [12].

$$Co(OAc)_2 + O_2 \rightarrow Co^{III}(O_2^{-\bullet})(OAc)_2 \quad (1)$$

$$Co(OAc)_2 + ROOH\,(\text{trace}) + HOAc \rightarrow Co(OAc)_3 + RO^{\bullet} + H_2O \quad (2)$$

The $Co(OAc)_3$ then reacts rapidly with $Mn(OAc)_2$ generating $Mn(OAc)_3$; $Co(OAc)_3$ is reduced to $Co(OAc)_2$ in the process

$$Co(OAc)_3 + Mn(OAc)_2 \rightarrow Co(OAc)_2 + Mn(OAc)_3 \quad (3)$$

The Mn(III) ion, in turn, abstracts an electron from Br^- generating the bromine radical, $Br^{\bullet}$ a crucial species which abstracts a hydrogen atom from a methyl group of PX and initiates the oxidation of *p*-xylene.

$$Mn(OAc)_3 + Br^- \rightarrow Mn(OAc)_2 + Br^{\bullet} + OAc^- \quad (4)$$

$$Br^{\bullet} + H_3CC_6H_5CH_3 \rightarrow HBr + H_3CC_6H_5CH_2^{\bullet} \quad (5)$$

$$H_3CC_6H_5CH_2^{\bullet} + ROOH \rightarrow H_3CC_6H_5CH_2OOH + R^{\bullet} \quad (6)$$

Cerium, probably, functions similar to manganese while nickel and zirconium can substitute for cobalt. This model is shown schematically in Fig. 8. This model is an extension of that proposed by Partenheimer [3,18,19]. The role of dioxygen in generating Co(III) species from Co(II) is supported by our electronic and EPR spectral results (Fig. 1(a) and Fig. 3).

Our electronic spectroscopic results (Fig. 1) show that in the system $Co/Mn/Br^-/HOAc/O_2/H_2O/PX$, Mn(III) cluster complexes could be detected in addition to $Co(OAc)_2$. It is also probable that $Co(OAc)_3$ and Co(OAc)Br are also present and are

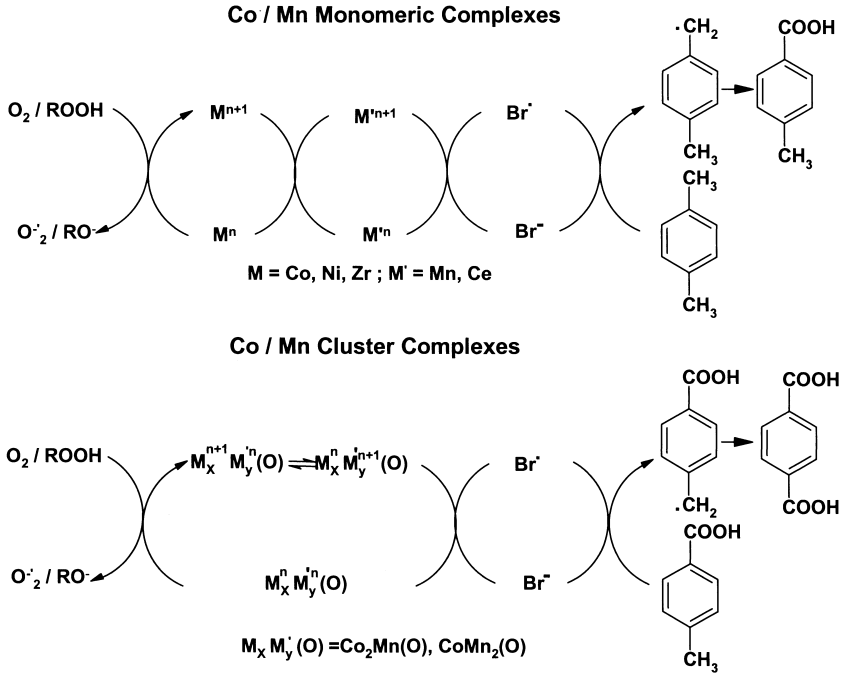

Fig. 8. Reaction pathways.

not seen due to their extremely short half-lives arising from their very high redox activities. The band at 630 nm in the electronic spectra (Fig. 1(a)) provides evidence for the formation of Co(III) species. The intensity of this band increases continuously during the course of the reaction indicating the enhanced formation of Co(III) species. However, in the presence of the substrate, PX or Mn(II) salt, this band corresponding to Co(III) is absent (Fig. 1(b)). It is probably consumed fast in the oxidation Mn(II) to Mn(III). The spectral bands at 460 and 350 nm (Fig. 1(c)) corresponding to monomeric and Mn(III) cluster complexes present during the reaction indicate that their half-life is relatively longer than that of Co(III) species. The presence of Mn(III) cluster complexes under reaction conditions is also supported by our EPR results (Figs. 3–5). More specifically, solutions with an excess of manganese (Co:Mn = 1:3) contain homonuclear $Mn_3(O)(OAc)_x$ type clusters (Scheme 1) as the major species with a minor component being $CoMn_2(O)(OAc)_x$ clusters (Fig. 4, Table 1). Solutions with an excess of cobalt (Co:Mn = 3:1 mmol) contain heteronuclear clusters of the type $Co_2Mn(O)(OAc)_x$ (Scheme 1) as a predominant species and $Co_3(O)(OAc)_x$ and $Mn_2Co(O)(OAc)_x$ (Scheme 1) as the minor ones. The cluster complexes showed a broad EPR signal below the free spin g value (2.0023) at 298 K. They became EPR silent at 77 K, probably due to antiferromagnetic interactions among the manganese atoms of the cluster. The presence of Zr(IV) ions enhanced the concentration of Mn(III) cluster complexes (Fig. 3) as well as the rate of oxidation of PX (Table 2). A similar enhancement in the cluster complex formation was observed also at higher Br^- concentrations (Fig. 5). The concentration of the cluster complexes was high in solutions with Co:Mn:Br^- mmol ratios of 3:1:6 (Fig. 5, curve (b)). The Mn(III) cluster complexes probably play a significant role in the oxidation of the bromide ion to bromine atom. When Co/Br or Mn/Br alone were used as the catalysts, the PX conversions are low (compared to systems containing both Co and Mn). More importantly, 4-CBA and TA are not observed among the products. The further oxidation of *p*-toluic acid to 4-CBA and TA is significantly enhanced by (1) the simultaneous presence of Co and Mn, (2) presence of Zr, and (3) optimal amounts of Br^- (Table 2). Spectroscopic

studies revealed that in the initial stages of the reaction, Co(III) and Mn(III) are present as monomeric species (Fig. 3(a) and 4(a)). Cluster complexes were observed only after 3–5 h. The comparative spectral and catalytic data (Tables 1 and 2) suggest that while monomeric complexes can abstract a hydrogen atom from the methyl group of PX (to form *p*-methylbenzyl radical which undergoes oxidation to *p*-toluic acid), the further oxidation of *p*-toluic acid is more difficult. The $p-\sigma^+$ Hammett substituent constant changes from -0.31 (for PX) to $+0.42$ (for *p*-toluic acid) [3]. The reduction in ring electron density results in the hydrogen abstraction from methyl group in *p*-toluic acid being 4.9 times slower [3]. Monomeric complexes, probably, cannot abstract a H atom from *p*-toluic acid. Cluster complexes are apparently required. Support for this hypothesis comes also from runs containing small quantities of zirconium as well as higher amounts of bromine (Runs 2A–2D, 6A and 14A). In these cases the spectroscopic data (Figs. 3 and 5) indicate that the cluster complexes $Co_2Mn(O)(OAc)_x$ and $CoMn_2(O)(OAc)_x$ are formed even at the start of the reactions leading to higher values of TOF and conversion of *p*-toluic acid to 4-CBA and TA. Although the present study does not evince, unequivocally, the exact compositions of the cluster complexes due to the complexity of the various species present in the homogeneous solutions, we propose that bimetallic clusters, like $Co_2Mn(O)(OAc)_x$ and $CoMn_2(O)(OAc)_x$, play a vital role in the oxidation of *p*-toluic to terephthalic acid. Preliminary work on the oxidation of *p*-toluic acid over these cluster complexes [38] supports this hypothesis.

4. Conclusion

The identities of the complexes of cobalt and manganese present during the aerobic oxidation of *p*-xylene at 363 K by the $Co/Mn/Br^-$ system in acetic acid solvent have been investigated by electronic and EPR spectroscopies as well as catalytic reaction techniques. Both the specific catalytic activity (turnover frequency, TOF) for *p*-xylene conversion and the yield of terephthalic acid are enhanced by (1) the presence of both cobalt and manganese in the catalyst system, (2) additives like Zr and Ce, and (3) an optimal concentration of Br^-. The reaction mixtures contain, in addition to $Co(OAc)_2$ and $Mn(OAc)_2$, many additional species like Co(OAc)Br, $Co(OAc)_3$, $Co_3(O)(OAc)_x$, $Co_2Mn(O)(OAc)_x$ and $CoMn_2(O)(OAc)_x$. An interesting finding from our combined spectroscopic and catalytic studies is that the system exhibited high catalytic activity and yield of terephthalic acid when heteronuclear cluster complexes like $Co_2Mn(O)(OAc)_x$ and $CoMn_2(O)(OAc)_x$ were present in significant concentrations in the reaction mixture. The role of these complexes in the oxidation reaction is discussed.

Acknowledgements

The authors thank Drs. (Mrs.) Sarada Gopinathan, Seema Deshpande and Manju Deogaonkar for their help.

References

[1] US Patent No. 2,833,816 (1958).
[2] PCT Int. Appl. WO 9,931,038 A1 (24 June 1999).
[3] W. Partenheimer, Catal. Today 23 (1995) 69.
[4] Dioxygen Activation and Homogeneous Catalytic Oxidation, in: L.I. Simandi (Ed.), Elsevier, Amsterdam, Vol. 66, 1991.
[5] The Activation of Dioxygen and Homogeneous Catalytic Oxidation, in: D.H.R. Barton, A.E. Martell, D.T. Sawyer (Eds.), Plenum Press, New York, 1993.
[6] G.W. Parshall, S.D. Ittel, Homogeneous Catalysis, Wiley-Interscience, New York, 1992.
[7] G.R. Steinmetz, C.E. Sumner, J. Catal. 100 (1986) 549.
[8] Y. Kamiya, J. Catal. 33 (1974) 480.
[9] A.S. Hay, H.S. Blanchard, Can. J. Chem. 43 (1965) 1306.
[10] C.F. Hendricks, H.C.A. Van Beck, P.M. Heartjes, Ind. Eng. Chem. Prod. Res. Dev. 18 (1979) 38.
[11] M. Harustiak, M. Hrorec, J. Ilawky, J. Mol. Catal. 53 (1989) 209.
[12] W. Partenheimer, J. Mol. Catal. 67 (1991) 35.
[13] S.A.H. Zaidi, Appl. Catal. 27 (1986) 99.
[14] S.A.H. Zaidi, Appl. Catal. 42 (1988) 247.
[15] Y.G. Chuan, X. Zuwei, C. Guoying, F. Shuhua, H. Xiaodan, Appl. Catal. A. General 185 (1999) 277.
[16] US Patent Nos. 4,786,753 and 5,453,538.
[17] Catalytic Oxidation: Principles and Applications, in: R.A. Sheldon, R.A. Van Santen (Eds.), World Science, Netherlands Institute for Catalysis Research, Singapore, 1995.

[18] W. Partenheimer, J.A. Kaduk, Stud. Surf. Sci. Catal. 66 (1991) 613.
[19] R.K. Gipe, W. Partenheimer, Stud. Surf. Sci. Catal. 110 (1997) 1117.
[20] G.H. Jones, J. Chem. Res.(S) (1982) 207.
[21] G.H. Jones, J. Chem. Soc., Chem. Commun. (1979) 536.
[22] E. Konbek, J.O. Edwards, J. Inorg. Nucl. Chem. 25 (1963) 1401.
[23] C.E. Sumner Jr., Inorg. Chem. 27 (1988) 1320.
[24] C.E. Sumner, G.R. Steinmetz, J. Am. Chem. Soc. 107 (1985) 6124.
[25] J.I. Ziolkowski, F. Pruchnik, T. Szymanska-Buzar, Inorg. Chim. Acta 7 (1973) 475.
[26] B.R. McGarvey, in: R.L. Carlin (Ed.), Transition Metal Chemistry, Marcel Dekker, New York, Vol. 3, 1968, p. 89.
[27] A.B.P. Lever, Inorganic Electronic Spectroscopy, Elsevier, Amsterdam, 1968.
[28] H.A. Kuska, M.T. Rogers, in: A.E. Martell (Ed.), Coordination Chemistry, Van Nostrand Reinhold, New York, Vol. 1, 1971, p. 186.
[29] S. Deshpande, D. Srinivas, P. Ratnasamy, J. Catal. 188 (1999) 261.
[30] J.B. Vincent, H.-R. Chang, K. Folting, J.C. Huffman, G. Christou, D.N. Hendrickson, J. Am. Chem. Soc. 109 (1987) 5703.
[31] J.K. McCusker, G.Ho. Jang, S. Wang, G. Christou, D.N. Hendrickson, Inorg. Chem. 31 (1992) 1874.
[32] R.D. Cannon, R.P. White, Prog. Inorg. Chem. 36 (1988) 195.
[33] E. Suresh, M.M. Bhadbhade, K. Venkatasubramanian, Polyhedron 16 (1997) 3941.
[34] J. K Beattie, T.W. Hambley, J.A. Klepetko, A.F. Masters, P. Turner, Polyhedron 15 (1996) 2141.
[35] G.M. McGarvey, in: R.L. Carlin (Ed.), Transition Metal Chemistry, Marcel Dekker, New York, Vol. 3, 1968, p. 89.
[36] J.N. Van Niekerk, F.R.L. Schoening, Acta Crystallogr. 6 (1953) 609.
[37] E.F. Bertant, T. Qui Due, P. Burlet, P. Burlet, M. Thomas, J.M. Moreau, Acta Crystallogr. 30B (1974) 2234.
[38] S.A. Chavan, S.B. Halligudi, D. Srinivas, P. Ratnasamy, unpublished results.